SECOND EUROPEAN CONFERENCE ON EARTHQUAKE ENGINEERING
AND SEISMOLOGY, ISTANBUL AUG. 25-29, 2014

# SIMULATION OF OUT-OF-PLANE INSTABILITY IN RECTANGULAR RC STRUCTURAL WALLS

Farhad DASHTI[1], Rajesh P DHAKAL[2] and Stefano PAMPANIN[3]

## ABSTRACT

Out-of-plane instability is identified as one of the common failure modes of slender rectangular RC walls. This mode of failure was previously observed in experimental studies of rectangular walls, and has attracted more attention following the out-of-plane failures of several walls in the recent earthquakes in Chile and Christchurch.

In this study, out-of-plane instability of slender rectangular walls subject to in-plane loading is simulated using finite element analysis. Experimental results of a cantilever wall specimen which failed in out-of-plane mode were used for verification of the modelling and analysis. The FEM analysis was carried out using the software DIANA. Curved shell elements with embedded bar elements were used to simulate the reinforced concrete section. This type of model does not require 'plane sections to remain plane' along a wall, and simulates the in-plane axial-flexure-shear interaction without any empirical adjustment. The model is found to be capable of predicting the out-of-plane instability observed during the test and could capture cyclic response of the specimen reasonably well in terms of global parameters such as lateral load-top displacement curves and local parameters as nonlinear strain profile at the wall base. Also, development of the out-of-plane deformation in different regions of the wall is scrutinized using detailed response of the reinforcement and concrete elements positioned along the wall thickness at different stages of the failure mode.

## INTRODUCTION

The structural wall system was introduced in the 1970s, and design provisions for this system have evolved since then. However, recent earthquakes in Chile ($M_w$ 8.8, February 2010) and New Zealand (February 2011, $M_L$=6.3) revealed the fact that despite having been investigated for many years, shear walls still have some issues that should be resolved to ensure their satisfactory performance in relatively severe earthquakes. In the recent earthquakes, structural wall damage included concrete crushing in the boundary zones, reinforcement fracture, and global wall buckling. Some of the failures are attributable to lack of closely spaced transverse reinforcement at wall boundaries, which was not required by the Chilean code based on the good performance of buildings in the 1985 $M_{7.8}$ earthquake. However, many of the failures observed in the 2010 Chile earthquake are not yet understood, and indicate that there are deficiencies in current US design provisions (Massone and Wallace 2011, Wallace 2011). In some cases, lateral instability (buckling) of a large portion of a wall section was

[1] PhD Candidate, Department of Civil and Natural Resources Engineering, University of Canterbury, Christchurch, New Zealand, farhad.dashti@pg.canterbury.ac.nz
[2] Professor, Department of Civil and Natural Resources Engineering, University of Canterbury, Christchurch, New Zealand, rajesh.dhakal@canterbury.ac.nz
[3] Professor, Department of Civil and Natural Resources Engineering, University of Canterbury, Christchurch, New Zealand, stefano.pampanin@canterbury.ac.nz

observed (Figure 1). Prior to the Chile earthquake, this global buckling failure had only been primarily observed in laboratory tests (Oesterle 1979, Vallenas et al. 1979, Goodsir 1985, Thomsen IV and Wallace 2004, Johnson 2010) (Figure 2).

According to Telleen et al. (2012a), "Overall wall buckling refers to the buckling of a portion of a wall section out-of-plane (as opposed to buckling of individual reinforcing bars), as a result of in-plane wall flexure during an earthquake. The buckling is typically limited to an end region of the wall where vertical tension and compression strains from in-plane wall flexure are greatest." This mode of failure was also observed in recent tests of single structural wall specimens in the US and tests of two full-scale 4-story buildings with high-ductility structural walls (Tuna et al. 2012) even though they complied with building code provisions and recommendations of ACI and AIJ. Negae et al (2011) summarized important details of the two 4-story buildings tested in E-Defense, one being conventionally reinforced and the other using high-performance RC construction, both with rectangular walls (Figure 3 (a)). The conventionally reinforced wall had confinement exceeding US requirements, with axial load of approximately 0.03Agf'c; yet the compression boundary zone sustained localized crushing and lateral buckling (Figure 3 (b)), under the input record of Kobe 100% (Wallace 2012).

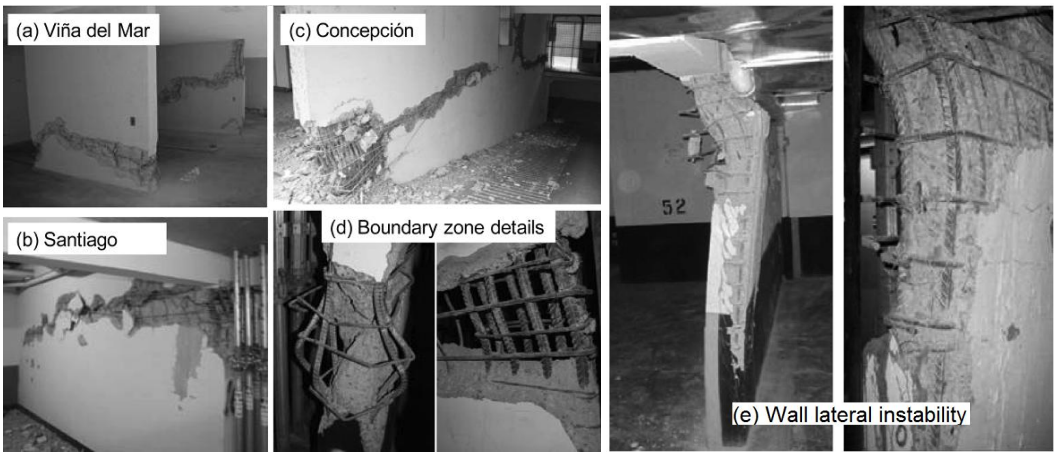


Figure 1. Typical wall damage in 2010 Chile earthquake (Wallace 2012)

a) b)

Figure 2. Wall damage in laboratory tests, a) Goodsir (1985) b) Johnson (2010)

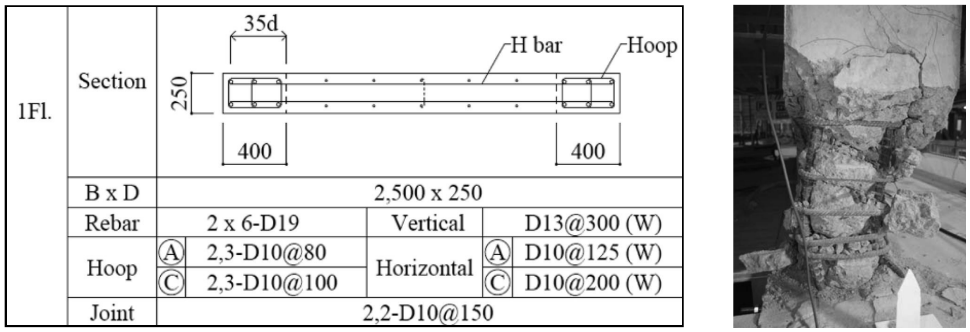


a) b)

Figure 3. E-Defense shaking table test on conventionally reinforced 4-story shear wall building: a) Wall plan. b) Wall damage (Wallace 2012).

The 2011 Christchurch earthquake showed many similar wall failures, suggesting the deficiencies observed in the 2010 Chile earthquake are not one-off. According to the EERI special earthquake report on the Christchurch, New Zealand, earthquake of February 22 (2011) the Special Issue of the Bulletin of the NZSEE (Kam et al, 2011) and the Canterbury Earthquakes Royal Commission Reports (2012), structural walls did not perform as anticipated. Boundary zone crushing and bar buckling were observed mostly in Pre-1970s RC walls which were generally lightly reinforced, were not detailed for ductility and had inadequate reinforcement to provide confinement to the concrete and buckling restraint to the longitudinal reinforcement.

On the other hand, modern (Post-1970s) RC wall buildings were observed to have experienced failure patterns like wall web buckling, boundary zone bar fracture and buckling failure of ducted splice. In a number of cases, compression failure occurred in the outstanding legs of T and L walls in addition to significant out-of-plane displacements, thereby resulting in overall buckling of the wall. Figure 4 shows the overall buckling of one outstanding leg of a V-shaped wall. Also, one of the walls of the Grand Chancellor Hotel of Christchurch experienced an out-of-plane brittle shear-axial failure at the ground floor level.. The failure plane initiated at the top of the lap splice in the web vertical reinforcement (Figure 5) and is more likely due to the combination of in-plane and out-of plane (bi-directional) loading.

As noted above, out-of-plane instability of slender rectangular walls has been observed in several cases in recent earthquakes causing concerns over the existing design provisions of walls. This study investigates the causes and consequences of this mode of failure using a micro-model based finite element analysis.

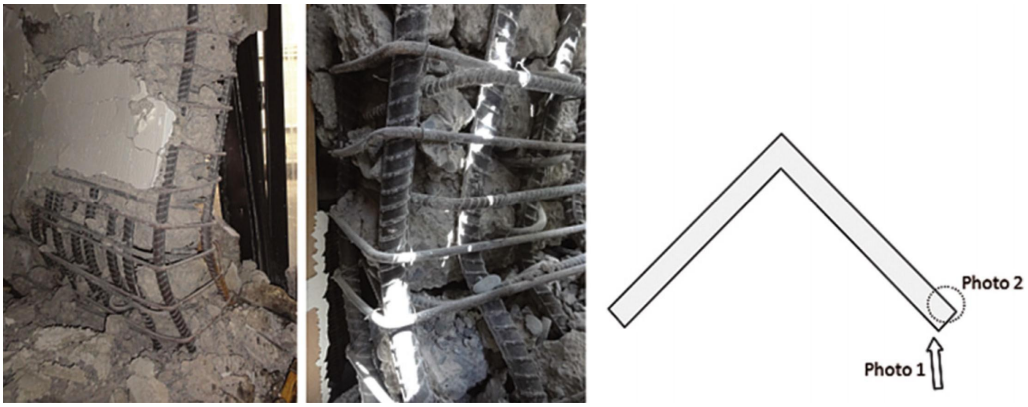


Figure 4. Web buckling of well-confined wall (Elwood 2013)

Figure 5. Failure of wall D5-6 of the Grand Chancellor Hotel (Kam et al. 2011)

## MODEL DESCRIPTION

In this study, finite element analyses were carried out using DIANA9.4.4 (DIANA 2011). Curved shell elements with embedded bar elements were used to simulate RC walls. The curved shell elements in DIANA (Figure 6) can be used for capturing buckling and postbuckling responses based on isoparametric degenerated solid approach by introducing two shell hypotheses (DIANA 2011):

- Straight-normals: this hypothesis assumes that normals remain straight, but not necessarily normal to the reference surface. Transverse shear deformation is included according to the Mindlin-Reissner theory (Reissner 1945, Mindlin 1951).
- Zero-normal-stress: It assumes that the normal stress component in the normal direction of a lamina basis is forced to zero: $\sigma_{zzl}(\xi,\eta,z) = 0$. The element tangent plane is spanned by a lamina basis which corresponds to a local Cartesian coordinate system ($x_l$, $y_l$) defined at each point of the shell with $x_l$ and $y_l$ tangent to the ($\xi$, $\eta$) plane and $z_l$ perpendicular to it.

In the curved shell elements, the in-plane lamina strains $\varepsilon_{xx}$, $\varepsilon_{yy}$ and $\gamma_{xy}$ vary linearly in the thickness direction unlike in flat shell elements where the integration is only performed in the reference surface. The transverse shear strains $\gamma_{xz}$ and $\gamma_{yz}$ are forced to be constant in the thickness direction. Since the actual transverse shearing stresses and strains vary parabolically over the thickness, a shear correction factor is applied using the condition that a constant transverse shear stress yields approximately the same shear strain energy as the actual shearing stress.

Five degrees of freedom are defined in every element node: three translations and two rotations. Further characteristics of the curved shell elements are: 1) They must be thin, i.e., the thickness 't' must be small in relation to the dimension b in the plane of the element; 2) Force 'F' may act in any direction between perpendicular to the surface and in the surface; and 3) Moment 'M' should act around an axis which is in the element face.

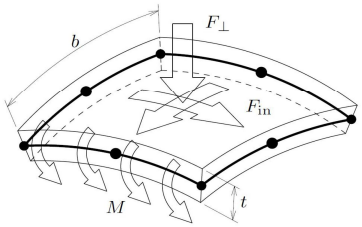


Figure 6. Curved shell element (DIANA 2011)

## Concrete stress-strain relationship

The Total Strain Crack Model available in DIANA (DIANA 2011) is used to represent the behaviour of the concrete elements. The constitutive model based on total strain is developed along the lines of the Modified Compression Field Theory, originally proposed by Vecchio & Collins (1986). As per the multi-directional fixed crack model, the total strain based crack models follow a smeared approach for the fracture energy. One of the main advantages of this model over the other concrete models in DIANA is that its basic properties can be derived from Model Code regulations for concrete, or they may be input directly. By default, DIANA assumes appropriate values for the various parameters describing the constitutive behavior. The axial stress-strain data captured using Popovics/Mander`s constitutive model (Mander et al. 1988) (Figure 7a) was implemented in the Total Strain Rotating Crack model to incorporate the confined concrete properties in the boundary elements and behavior of the unconfined portion was modeled using the axial stress-strain relationship of unconfined concrete.

## Reinforcement stress-strain relationship

The reinforcing bars are modelled using embedded reinforcement approach available in the program (DIANA 2011). In this approach, reinforcement elements are embedded in the structural elements, the so-called mother elements. DIANA ignores the space occupied by the embedded reinforcing bars; the mother element neither diminishes in stiffness, nor in weight. The reinforcement does not contribute to the weight (mass) of the element. Standard reinforcement elements do not have degrees of freedom of their own. In standard reinforcement, the strains are computed from the displacement field of the mother elements. This implies perfect bond between the reinforcement and the surrounding concrete. The stress-strain curve of the reinforcing steel is defined using Menegotto and Pinto (1973) model (Figure 7b). Bar buckling is not included in this constitutive model, hence the effect of bar buckling is neglected in the analysis.

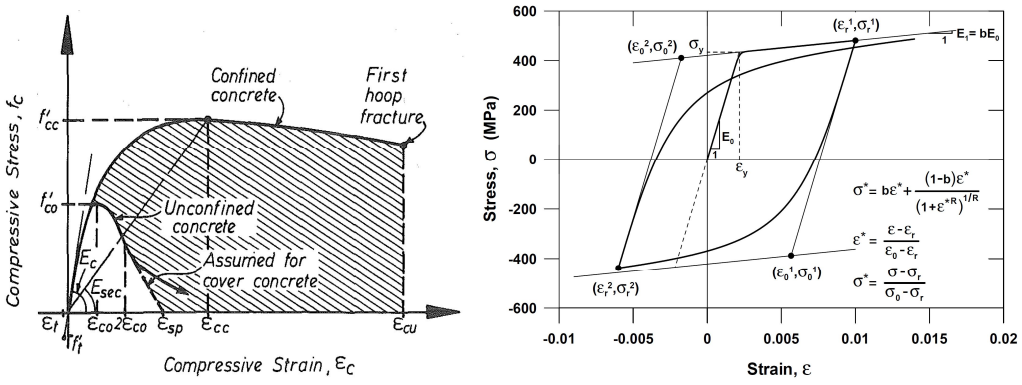


a) Concrete b) Steel

Figure 7. Constitutive models of materials

## EXPERIMENTAL VERIFICATION

One of the cantilever wall specimens tested by Oesterle (1976) at Portland Cement Association Construction Technology Laboratories is used for verification in this study. The specimens were approximately 1/3-scale representations of full-size walls, although no specific prototype walls were modelled. Each specimen was loaded as a vertical cantilever with lateral force applied through the top slab, and no axial load was applied to the specimens. Specimen R2 was chosen for experimental verification. This specimen was a rectangular shaped wall with 4.0% vertical reinforcement concentrated within a distance of 7.5 in. (190.5 mm) from each end. The boundary element had confinement reinforcement in the lower 6 ft (1.83 m) of the boundary elements (Oesterle 1976). Dimensions and reinforcement layout of the specimen as well as the finite element model are shown in Figure 8. The specimen was subjected to 39 displacement cycles at the top level as per the loading history shown in Figure 9, and no axial load was applied. Figure 8c displays the loading direction as

well as the boundary conditions applied to the model. The top nodes were constrained against translation in the out-of-plane direction. It should be noted that the mesh size was chosen after a mesh sensitivity analysis. Figure 10 displays the key milestones of the wall response observed during the test.

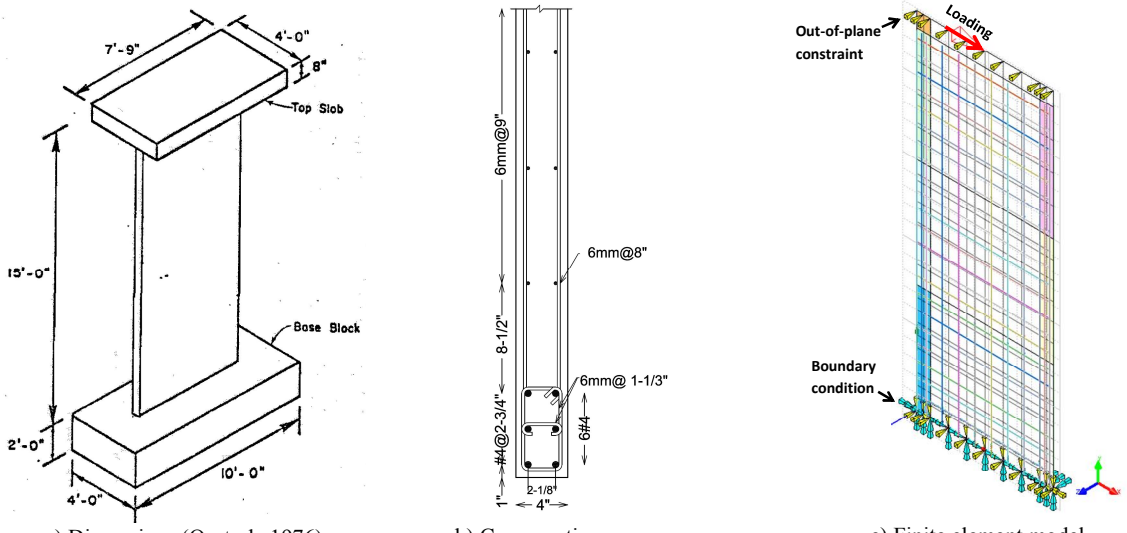


a) Dimensions (Oesterle 1976) b) Cross section c) Finite element model

Figure 8. Wall specimen R2 (1 ft = 0.30 m; 1in. = 25.4 mm)

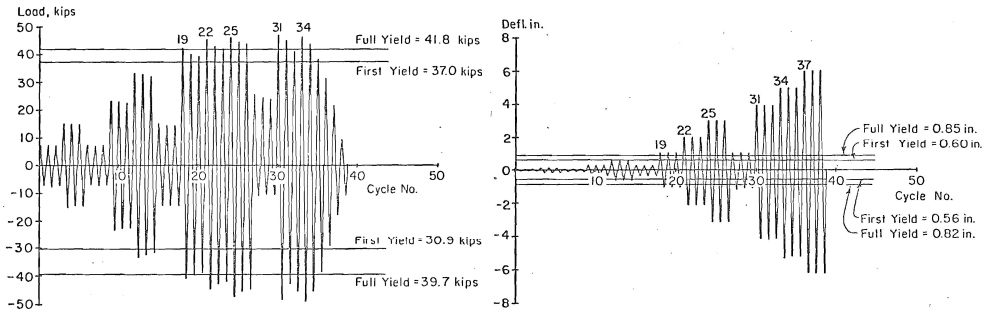


a) b)

Figure 9. Loading history for the specimen (Oesterle 1976): a) Load History, b) Deflection History (1 in. = 25.4 mm; 1 kips = 4.448 kN)

Figure 11a compares the predicted wall response with the experimental measurements, and Figure 11b shows vertical displacement of the mid-length node at the top level of the wall, which shows elongation and instability of the wall model at the final load cycles. The points corresponding to the key milestones of the analytical results are shown in this figure with the corresponding values compared with the experimental measurements given in Table 1. The model could reasonably predict the points corresponding to cracking and yielding of the material at different stages of loading. In particular, the ability of the analysis to capture the out-of-plane deformation in the compression boundary zone despite being subjected to pure in-plane action is very encouraging. In the authors` knowledge, this has been achieved for the first time.

Figure 12 displays the steel strain measurements of the specimen at wall base in comparison with the model predictions at the positive peak of selected drift cycles applied during testing. Due to a gage malfunction the measurements were taken up to 0.56% drift in some parts and 1.1% drift at the tension boundary element. The nonlinear strain gradient along the length of the wall which is usually neglected in simplified analysis methods is predicted by the analysis with a relatively good agreement

with the measured steel strain profile. As shown in Figure 12, although the bond-slip effect is not considered in the analysis, the agreement between the predicted strain profile of the wall section and strain measurements of the reinforcement in the test is reasonable. The strain profile at 1.1% drift level follows the same trend as the one at 0.56% drift level, but understandably with considerably greater strain values. The predicted neutral axis position matched well with test results as well.

According to the test report, during Cycle 28, a 1 in. (25.4 mm) deflection cycle after the 3in. cycles, bowing of the compression end was observed. The compression boundary element was 0.25 in. (6.4 mm) out-of-plane at a point 3.5 ft (1.1 m) above the base. Although this bowing progressed further with each cycle, the load carrying capacity of the wall remained stable. An omni-direction ball caster was placed against the face of each boundary element at 3.5 ft (1.1 m) above the base. This simulated lateral support at approximately the first story height. The test was continued with the 4 in. (101.6 mm) deflection cycle. Considerable out-of-plane deformation was observed during the 5 in. (127 mm) deflection cycles, which progressed further until the severe strength drop in the 6 in. deflection cycle.

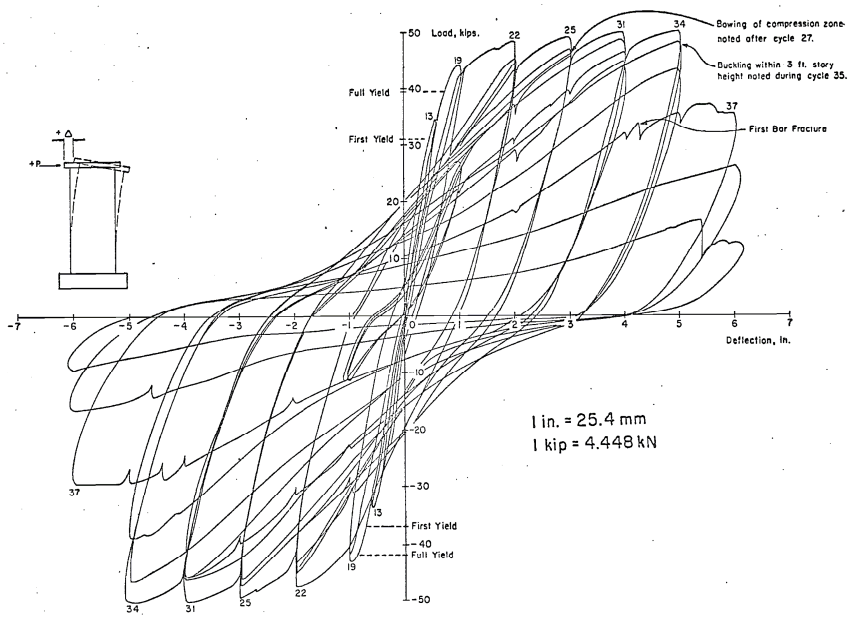


Figure 10. Load-deflection response of the specimen (Oesterle 1976)

In the analysis, considerable out-of-plane deformation was observed at 4$^{1}/_{3}$ ft (1321mm) above the base during the 4 in. (101.6 mm) displacement cycle while reversing from the +4in peak and approaching towards the -4in peak. The analysis continued until reaching +5.6 in. (142 mm) displacement in the +6in. (152.4 mm) cycle. At this level the out-of-plane deformation was big enough to stop the analysis. The instability of the model at different stages of loading due to out-of-plane deformation is further indicated in Figure 11b. For example, Point F, which corresponds to initiation and development of out-of-plane instability, does not induce any degradation in the lateral load-top displacement response of the specimen as shown in Figure 11a. This can be attributed to the fact that out of plane deformation results in earlier closure of the cracks in compression part of the section contributing to load carrying capacity of the wall. However, this effect is well illustrated in Figure 11b in which Point F (initiation of out-of-plane deformation) corresponds to a sudden considerable drop in the top vertical displacement. This drop is recovered by the concrete elements located on the compression side of the buckled section while approaching to Point G where the out-of-plane deformation is considerably larger. A similar trend is observed in the following cycle but with a considerable degradation at Point G (top displacement = -127 mm, Figure 11) and failure of the model at Point H (Figure 11). The degradation and failure of the model can be attributed to inability of the concrete elements to undertake further compression after reaching the ultimate strain capacity.

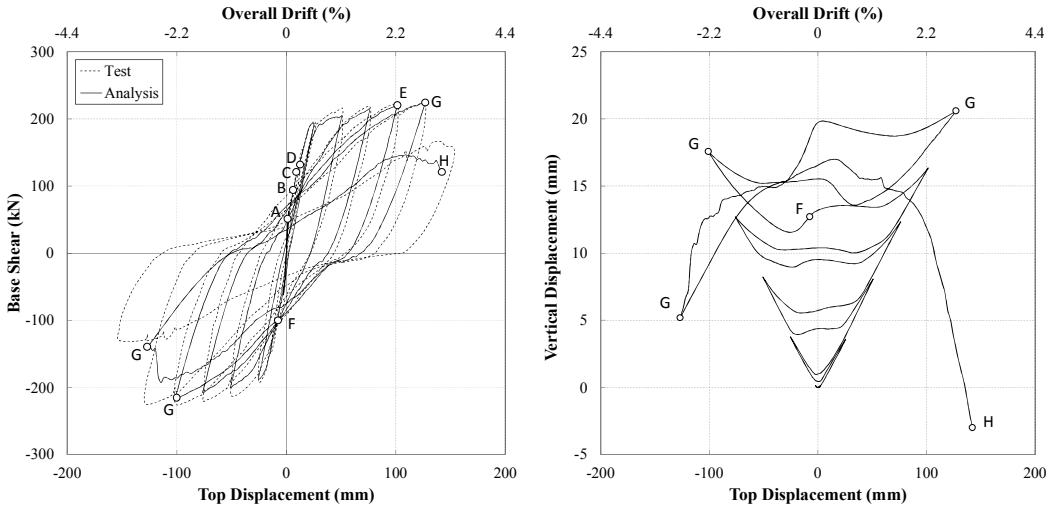


a) b)

Figure 11. Response of the specimen: a) Analytical versus experimental top displacement response b) Vertical displacement (uplifting due to plastic hinge elongation) at mid-length of the specimen

Table 1. Key milestones of specimen R2 response: numerical-experimental comparison

| | A: Initiation of Flexural Cracking | | B: Initiation of Inclined Cracking | | C: First Yield of Tension Reinforcement | | D: Tension Yielding of All Boundary Element Reinforcement | |
|---|---|---|---|---|---|---|---|---|
| | Test | Analysis | Test | Analysis | Test | Analysis | Test | Analysis |
| $F_H$(kN) | 67 | 51 | ----- | 94 | 165 | 121 | 186 | 132 |
| Drift(%) | 0.06 | 0.03 | ----- | 0.14 | 0.33 | 0.2 | 0.47 | 0.28 |
| | E: Concrete Reaching Maximum Strength at the Base | | F: Initiation of Out-of-Plane Deformation | | G: Considerable Out-of-Plane Deformation | | H: Ultimate Point | |
| | Test | Analysis | Test | Analysis | Test | Analysis | Test | Analysis |
| $F_H$(kN) | ---- | 221 | ---- | -67 | 209 | -215 | ---- | 121 |
| Drift(%) | ---- | 2.22 | ---- | 0.3 | 2.8 | -2.2,±2.8 | ----- | 3.1 |

$F_H$: Lateral Load

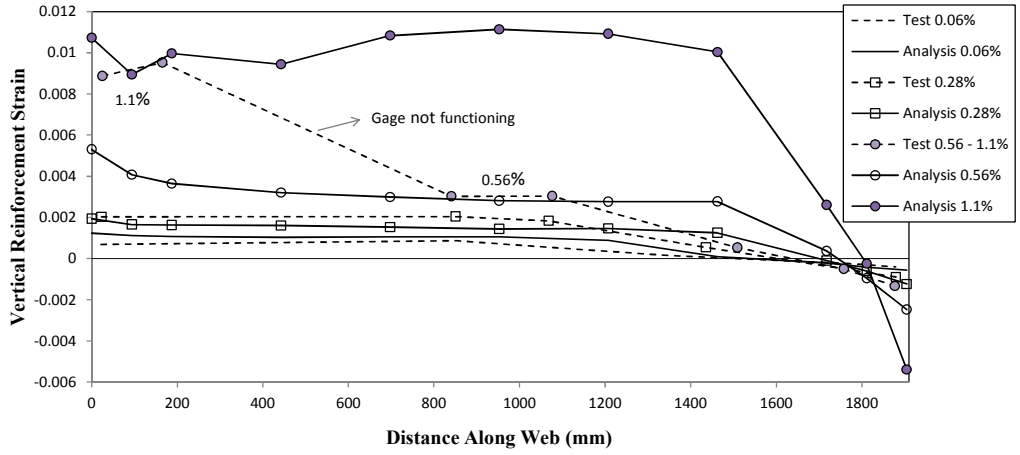


Figure 12. Variation of the vertical reinforcement strain along the wall length

In order to further investigate the formation of this instability, the points corresponding to the development of the out-of-plane deformation in the 4in (101.6 mm) cycle are shown in Figure 13, and the out-of-plane deformation of the model at these points is indicated with displacement values of the elements along the out-of-plane direction in Figure 14. Also, Figure 15 displays the corresponding vertical strain profile of the reinforcement and concrete elements at the critical section where the out-of-plane deformation initiated (the strain profile is plotted for both faces of the wall). Wall faces as well as the loading direction are also displayed in Figure 15.

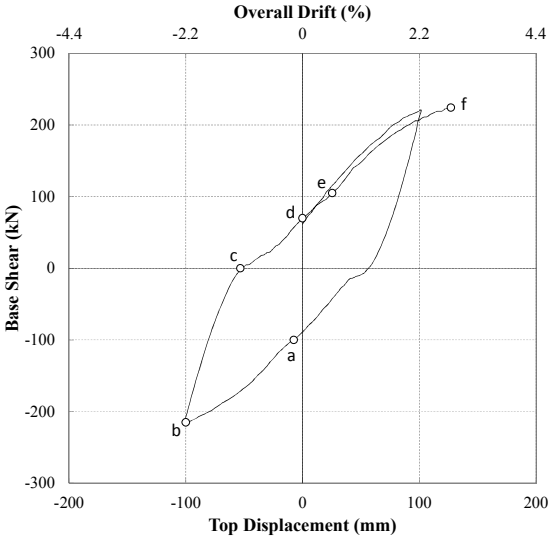


Figure 13. Initiation and development of the out-of-plane instability

In Figure 13, Point a corresponds to the initiation of the first considerable out-of-plane deformation (7.49 mm, shown in Figure 14a). At this point, the model has already reached the top displacement of +4in (2.2% drift) and is sustaining the top displacement of -0.3 in (0.2% drift). Figure 15 displays the considerable residual strain of the reinforcement and concrete elements remaining from the previous peak displacement. The previous tension side is under compressive stress at this point but the residual strain is large enough not to let the compression side experience a compressive strain until Point b which corresponds to -4in (-2.2% drift) top displacement when a considerable out-of-plane deformation has developed at the compression boundary element. The maximum out-of-plane displacement at this point is about 12 times greater than the one at Point a (Figure 14b). As shown in Figure 15, due to the out-of-plane deformation, strain profiles of the concrete and reinforcement elements depend on their position along the wall thickness with the outer layers (concrete layers) experiencing the extreme values. At Point b, even the concrete layer at Face 1 does not experience a considerable compression strain despite being under relatively greater compression force due to the out-of-plane deformation. At Point c (zero base shear and -1.3% drift, Figure 13) the maximum displacement of the model in the out-of-plane direction is still considerable (57 mm, Figure 14c) and the previous compressive strain of the concrete layer at Face 1 has changed to tensile strain in most of the compression side due to the decrease in out-of-plane displacement. Point d corresponds to zero top displacement (Figure 13). However, the strain profiles of the concrete and of the reinforcing bars are different throughout the wall length at this point indicating initiation of the out-of-plane deformation at the former tension side. The out-of-plane displacements and the corresponding material strains in the two boundary elements of the two extremes become similar to each other at Point e (Figure 14). Point f corresponds to +5in (127 mm) top displacement and 139 mm maximum out-of-plane displacement (Figure 14). The tension side undergoes a greater tensile strain at this point when compared to Point b and the compression side follows the same pattern as the one at Point b. As the out-of-plane displacement is about 50% greater at this point compared to Point b, the strain profiles vary considerably at the compression side depending on their position along the wall thickness.

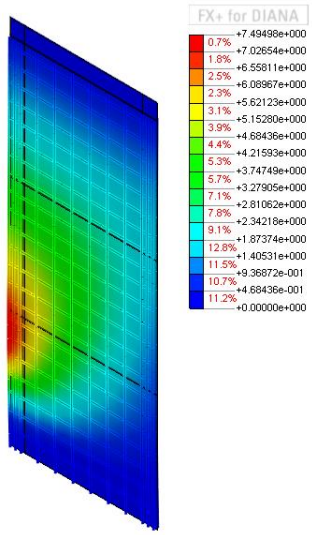


a) -0.2% Drift during 2.2% Drift Cycle

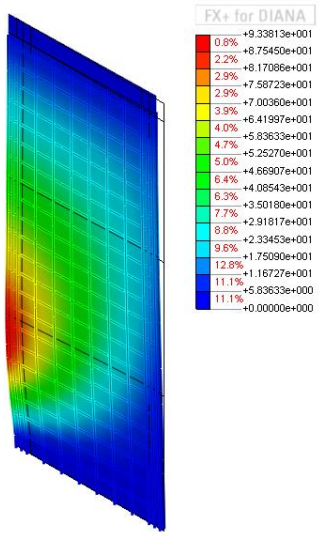


b) -2.2% Drift during 2.2% Drift Cycle

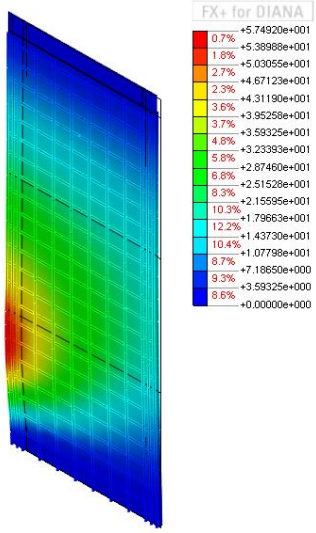


c) -1.3% Drift (Base Shear =0.0) reversing from -2.2% Drift

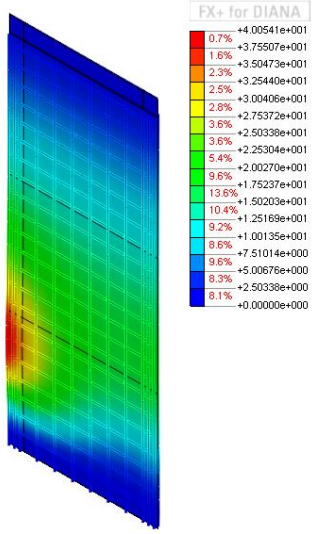


d) 0.0% Drift reversing from -2.2% Drift

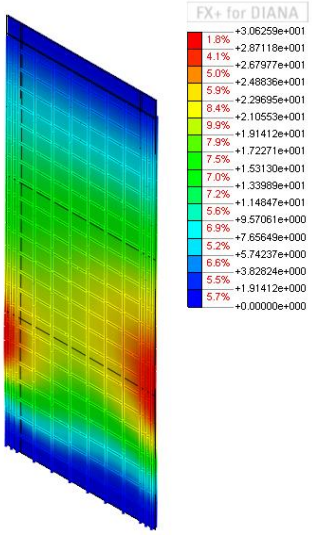


e) 0.4% Drift during 2.8% Drift Cycle

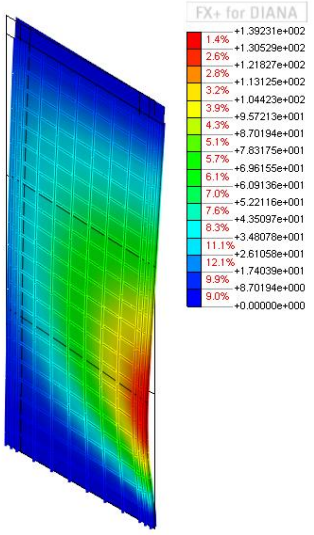


f) 2.8% Drift during 2.8% Drift Cycle

Figure 14. Out-of-plane deformation of the specimen (mm)

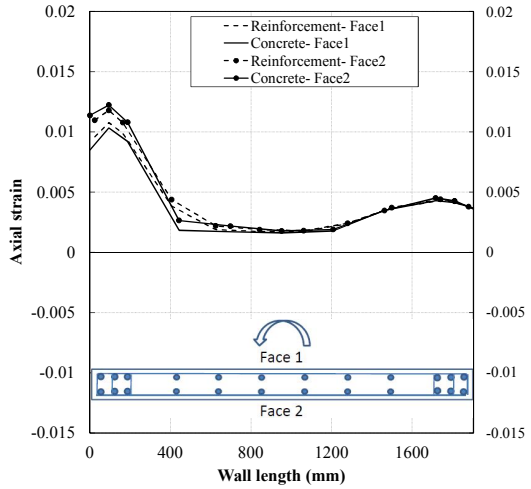


a) -0.2% Drift during -2.2% Drift Cycle

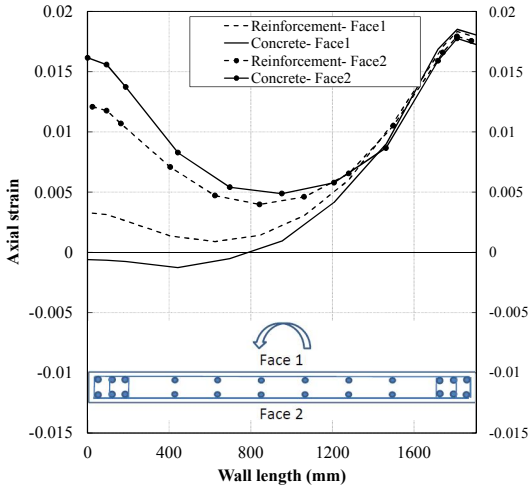


b) -2.2% Drift during 2.2% Drift Cycle

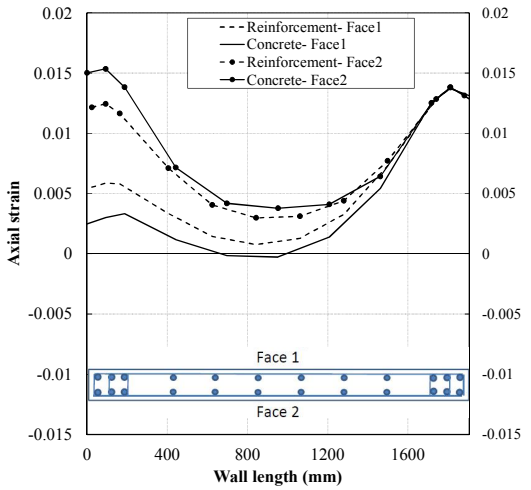


c) -1.3% Drift (Base Shear =0.0) reversing from -2.2% Drift

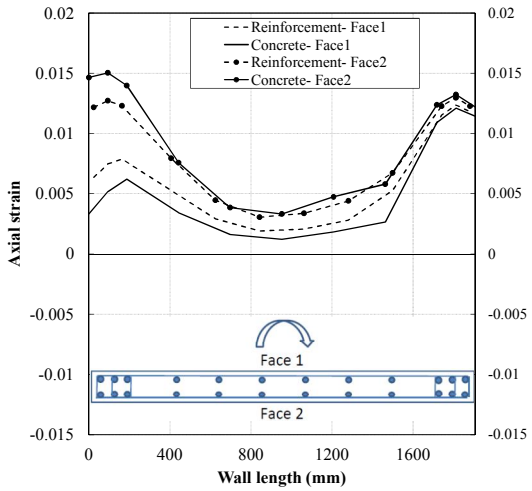


d) 0.0% Drift reversing from -2.2% Drift

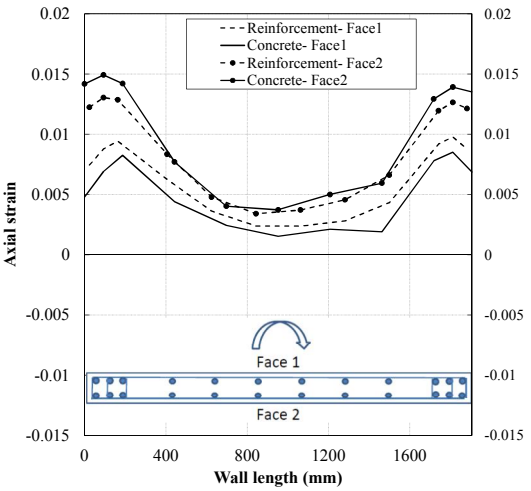


e) 0.4% Drift during 2.8% Drift Cycle

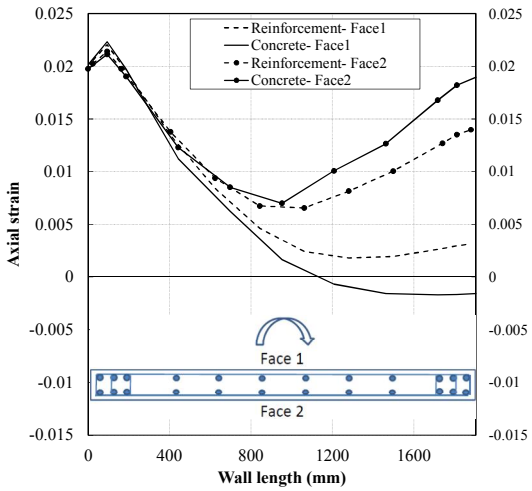


f) 2.8% Drift during 2.8% Drift Cycle

Figure 15. Vertical Strain gradient of the reinforcement and concrete elements at 4ft 4in (1321mm) level

## CONCLUSIONS

A finite element analysis approach using curved shell elements and embedded reinforcement elements in DIANA was used in this study to capture the out-of-plane failure of slender rectangular walls subject to in-plane loading.

The model could reasonably predict lateral load-top displacement response as well as the observed out-of-plane instability of a tested wall specimen. The wall height at which the maximum out-of-plane displacement developed was close to that observed in the test. The predicted key milestones of the wall response were in good agreement with the experimental results. The nonlinear strain profile at the wall base was also reasonably well predicted by the analysis.

Using this model, different stages in the progression of the out-of-plane instability could be investigated in detail, which contributed to better understanding of the causes and consequences of this common and important failure mechanism. Detailed investigation of the section behaviour corresponding to different stages of formation of out-of-plane deformation clearly shows the residual strain as one of the main parameters contributing to this failure mode.

A parametric study scrutinizing the effects of different parameters known to be influential in the formation of out-of-plane instability is undergoing by the authors with the aim to develop recommendations on different geometric and loading limitations to avoid this undesirable failure mode.

## REFERENCES


DIANA, T. (2011). Finite Element Analysis User's Manual - Release 9.4.4, TNO DIANA.

EERI (2011). "The M 6.3 Christchurch, New Zealand, Earthquake of February 22, 2011." *EERI Special Earthquake Report*.

Elwood, K. J. (2013). "Performance of concrete buildings in the 22 February 2011 Christchurch earthquake and implications for Canadian codes 1." *Canadian Journal of Civil Engineering* 40(3), 1-18.

Goodsir, W. J. (1985). The design of coupled frame-wall structures for seismic actions, University of Canterbury. PhD.

Johnson, B. (2010). Anchorage detailing effects on lateral deformation components of R/C shear walls, MasTer Thesis, UniversiTy of MinnesoTa.

Kam, W. Y., S. Pampanin and K. Elwood (2011). "Seismic performance of reinforced concrete buildings in the 22 February Christchurch (Lyttelton) earthquake." *Bulletin of the New Zealand Society for Earthquake Engineering* 44(4), 239-278.

Mander, J., M. N. Priestley and R. Park (1988). "Theoretical stress-strain model for confined concrete." *Journal of structural engineering* 114(8), 1804-1826.

Massone, L. and J. Wallace (2011). "Lessons from Chile: Impacts of Earthquake Engineering of RC Buildings in the US." *EERI/NEES Webinar*.

Menegotto, M. and P. Pinto (1973). Method of Analysis for Cyclically Loaded Reinforced Concrete Plane Frames Including Changes in Geometry and Non-elastic Behavior of Elements Under Combined Normal Force and Bending. IABSE Symposium on the Resistance and Ultimate Deformability of Structures Acted on by Well-Defined Repeated Loads, Lisbon.

Mindlin, R. D. (1951). "Influence of rotary inertia and shear on flexural motions of isotropic, elastic plates." *J. of Appl. Mech.* 18, 31-38.

Nagae, T., K. Tahara, T. Matsumori, H. Shiohara, T. Kabeyasawa, S. Kono, M. Nishiyama, J. Wallace, W. Ghannoum, J. Moehle, R. Sause, W. Keller and Z. Tuna (2011). Design and Instrumentation of the 2010 E-Defense Four-Story Reinforced Concrete and Post-Tensioned Concrete Buildings, Report.

NZRC (2012). "Canterbury Earthquakes Royal Commission Reports." http://canterbury.royalcommission.govt.nz/Final-Report-Volume-Two-Contents.

Oesterle, R. (1976). Earthquake Resistant Structural Walls: Tests of Isolated Walls, Research and Development Construction Technology Laboratories, Portland Cement Association.

Oesterle, R. (1979). Earthquake Resistant Structural Walls: Tests of Isolated Walls: Phase II, Construction Technology Laboratories, Portland Cement Association.

Reissner, E. (1945). "The effect of transverse shear deformation on the bending of elastic plates." *Journal of applied Mechanics* 12, 69-77.

Telleen, K., J. Maffei, J. Heintz and J. Dragovich (2012a). Practical Lessons for Concrete Wall Design, Based on Studies of the 2010 Chile Earthquake. 15th World Conference on Earthquake Engineering, 24-28 September 2012, Lisbon, Portugal.

Thomsen IV, J. H. and J. W. Wallace (2004). "Displacement-based design of slender reinforced concrete structural walls-experimental verification." *Journal of structural engineering* 130(4), 618-630.

Tuna, Z., S. Gavridou, J. Wallace, T. Nagae and T. Matsumori (2012). 2010 E-Defense Four-Story Reinforced Concrete and Post-Tensioned Buildings–Preliminary Comparative Study of Experimental and Analytical Results. 15th World Conference on Earthquake Engineering (15WCEE). Lisbon, Portugal.

Vallenas, J. M., V. V. Bertero and E. P. Popov (1979). Hysteretic behaviour of reinforced concrete structural walls. Report no. UCB/EERC-79/20, Earthquake Engineering Research Center, University of California, Berkeley.

Vecchio, F. J. and M. P. Collins (1986). "The modified compression-field theory for reinforced concrete elements subjected to shear." *ACI J.* 83(2), 219-231.

Wallace, J. (2012). "Behavior, design, and modeling of structural walls and coupling beams — Lessons from recent laboratory tests and earthquakes." *International Journal of Concrete Structures and Materials* 6(1), 3-18.

Wallace, J. W. (2011). February 27, 2010 Chile Earthquake: Preliminary Observations on Structural Performance and Implications for US Building Codes and Standards. ASCE Structures Congress, Las Vegas, ASCE.